Tailoring the photocurrent in BaTiO3/Nb:SrTiO3 photoanodes by controlled ferroelectric polarization

Maxime Rioult, Sukanya Datta, D. Stanescu, S. Stanescu, R Belkhou, F. Maccherozzi, Hélène Magnan, Antoine Barbier

Tailoring the photocurrent in BaTiO3/Nb:SrTiO3 photoanodes by controlled ferroelectric polarization

M. Rioult, S. Datta, D. Stanescu, S. Stanescu, R. Belkhou, F. Maccherozzi, H. Magnan, and A. Barbier

Citation: Applied Physics Letters **107**, 103901 (2015); doi: 10.1063/1.4930814
View online: http://dx.doi.org/10.1063/1.4930814
View Table of Contents: http://scitation.aip.org/content/aip/journal/apl/107/10?ver=pdfcov
Published by the AIP Publishing

Tailoring the photocurrent in $BaTiO_3$/Nb:$SrTiO_3$ photoanodes by controlled ferroelectric polarization

M. Rioult,[1] S. Datta,[1] D. Stanescu,[1] S. Stanescu,[2] R. Belkhou,[2] F. Maccherozzi,[3] H. Magnan,[1,a)] and A. Barbier[1]
[1]*Service de Physique de l'Etat Condensé, DSM/IRAMIS/SPEC, CEA-CNRS UMR 3680, CEA-Saclay, F-91191 Gif-sur-Yvette, France*
[2]*Synchrotron SOLEIL, L'Orme des Merisiers Saint-Aubin, 91192 Gif-sur-Yvette, France*
[3]*Diamond Light Source, Harwell Campus, Didcot, OX11 0DE Oxfordshire, United Kingdom*

(Received 6 July 2015; accepted 11 August 2015; published online 10 September 2015)

We demonstrate on prototypical samples containing a ferroelectric layer ($BaTiO_3$/Nb:$SrTiO_3$) that the efficiency of the system, used as photoanode, substantially depends on the polarization state of the ferroelectric layer. We show a significant increase of the photocurrent by a factor larger than 2 when the $BaTiO_3$ film is downward polarized. We explain this finding by the presence of an internal electric field which favors the separation of photo-generated charges. © *2015 AIP Publishing LLC*. [http://dx.doi.org/10.1063/1.4930814]

Abundant, cheap, and clean energy is the backbone of any modern civilization. As the decline of the fossil fuel era is yet foreseeable, it is important to change the impetus towards this global collapse. Hydrogen based energy harvesting, conversion, and storage is a promising technology. Hydrogen used in fuel cells produces only water as byproduct in comparison to the cocktail of carbon dioxide and other fine particles released on burning fossil fuels. Yet one of the bottlenecks is the fact that the methods currently available to produce hydrogen are not totally environment friendly as they involve a good deal of hydrocarbon burning or complex device design. Photoelectrolysis of water using sunlight is one of the most suitable methods for producing hydrogen with the important advantage of being environment friendly.[1–3] Unfortunately, the performance of conventional photoanodes is limited due to low absorption coefficient and a short hole diffusion length.[4] This problematics is common with photovoltaic applications.

In order to overcome these limitations, ferroelectric materials have been recently investigated as promising candidates for photoelectrodes and photovoltaic materials.[5] In ferroelectric based photovoltaic devices, the spontaneous polarization electric field is the driving force behind the photocurrent improvement.[6] The impact of ferroelectricity in the framework of photocatalytic applications has also been studied.[7] In particular, it has been proposed that the screening of the internal polarization induces band bending at the surface which favors oxidation (respectively, reduction) reactions in the case of an internal polarization pointing towards (respectively, outwards) the substrate.[8–10] In the case of $BaTiO_3$/TiO_2 structures, Burbure *et al.* reported that the internal electric field in the ferroelectric $BaTiO_3$ drives the band bending in the semiconducting TiO_2 and creates different spatial sites for oxidation and reduction reactions at the surface of TiO_2.[11] The potential use of such materials in the framework of water splitting through photoelectrolysis, even if less studied, is as well very promising.[7,12–14] However experimentally, assessing unambiguously the influence of the electric polarization is tricky because it is difficult to master the electric polarization in large size samples that need to be continuous and flat with a very well controlled crystallographic and chemical structure.

In the present work, we report on the substantial increase in the photoanode efficiency upon the polarization state of a prototypical ferroelectric $BaTiO_3$ upper layer. Our single crystalline systems, allowing a high level of control and high stability of the remnant polarization, are well suited for studying the influence of the ferroelectricity on the system material properties. Bulk $BaTiO_3$ is a ferroelectric material at room temperature exhibiting a para- to ferro-electric phase transition at about 130 °C accompanied by a cubic to tetragonal structural transition. The electrical polarization orientation lies along the (001) tetragonal axis.[15] The transition temperature increases fairly for strained epitaxial $BaTiO_3$ layers.

The $BaTiO_3$ epitaxial layers were deposited on single crystalline 1 at. % Nb:$SrTiO_3$ (001) substrates using atomic oxygen assisted molecular beam epitaxy (AO-MBE), a technique that makes possible the deposition of single crystalline layers of controlled morphology, stoichiometry and thickness.[16] The oxide layers were formed by evaporating high purity metals by thermal evaporation from Knudsen cells (deposition rate ~ 0.15 nm/min), while exposing the sample to atomic oxygen plasma (350 W) in an ultra-high vacuum vessel (10^{-7} mbar working conditions, 10^{-10} mbar base pressure). In order to have a homogeneous deposition and to reach the expected stoichiometry, the samples are rotated continuously around their surface normal during the deposition while kept at a temperature of 450 °C. The quality of the growing layers was monitored by *in situ* reflection high-energy electron diffraction (RHEED) (see supplementary material, Fig. S1).[17] Upon growth, the patterns evolve from typical features for single $SrTiO_3$ crystals to $BaTiO_3$ thin films ones, the final layers are single crystalline as cross-checked by transmission electron microscopy.[18] *In situ* XPS

a)Author to whom correspondence should be addressed. Electronic mail: helene.magnan@cea.fr

spectra of the Ba-*3d*, Ti-*2p* and O-*1s* core levels using Al K_α radiation were systematically recorded just after deposition to check the $BaTiO_3$ layer stoichiometry that was consistent with the previous reports.[16]

The photoelectrochemical (PEC) response of the samples was studied using a three electrodes cell with a quartz window.[4] The samples are mounted as the working electrode. Due to the piezoelectric character of the $BaTiO_3$ layer, special care was taken in order to prevent any kind of mechanical strain on the sample. A Pt wire and a Ag/AgCl electrodes were the counter and the reference electrodes, respectively, and a 0.1 M NaOH solution (pH = 13) was used as electrolyte. The I(*V*) measurements were carried out with a scan rate of 50 mV/s. The potential is reported *vs* the reversible hydrogen electrode (RHE) (V *vs* RHE = V *vs* Ag/AgCl + 0.197 + 0.06 pH). The light source is a 1000 W Xenon arc lamp with an infrared (IR) water filter. The chopped light (~0.5 s ON and ~0.5 s OFF) is obtained with a manual shutter. The intensity of the light on the sample was determined to be around 100 mW/cm^2. All PEC measurements were performed at room temperature.

To study the effect of the electric polarization on the photocurrent, the $BaTiO_3$/Nb:$SrTiO_3$ sample was macroscopically poled in an electrochemical cell (EC-poling) containing two electrodes and a non-aqueous electrolyte (0.1 M $LiClO_4$ in propylene carbonate) with a large electrochemical window.[19] The sample was mounted as the working electrode and a Pt wire as the counter electrode. Potentials of +8 V and −8 V were applied 2 or 3 times on the platinum counter electrode (during 10 s each), the last one being +8 V in order to obtain a remnant polarization pointing towards the substrate (downward polarization). During the procedure, the current was kept below 1 mA.

Figure 1 shows PEC measurements done on unpoled and +8 V EC-poled 25 nm $BaTiO_3$/Nb:$SrTiO_3$(001). We observe a more than two times increase of the photocurrent (defined as the difference between On and Off current densities) in the EC-poled sample, as compared to the unpoled one. Moreover, the onset potential for the EC-poled sample is significantly reduced by ~0.2 V. We checked the stability of our samples against photocorrosion by measuring

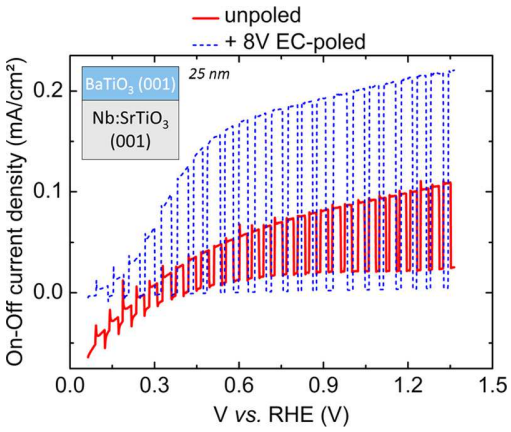

FIG. 1. On-off current density *versus* applied voltage curves *vs* RHE for unpoled (red solid line) and +8 V EC-poled (downward polarized) (blue dashed line) 25 nm $BaTiO_3$/Nb:$SrTiO_3$ (001).

photocurrent cycles during 30 min (Fig. S2). In order to investigate the eventual alteration of the $BaTiO_3$ layer upon EC-poling, we measured XPS before and after poling and observed no changes. Moreover, it has been reported that the sole Nb:$SrTiO_3$ single crystals show a substantial photocurrent.[20] We checked that EC-poling of our bare Nb:$SrTiO_3$ substrate induce no change in its PEC response. Thus, these results clearly show that the increase of the photocurrent on the $BaTiO_3$/Nb:$SrTiO_3$ sample after EC-poling originates only from a modification of the $BaTiO_3$ electrical polarization after EC-poling. Importantly, the effect of the polarization on the photocurrent reported here is much stronger than what was previously observed by Ji *et al.* in the case of ferroelectric $BiFeO_3$ photoanodes.[12]

The ferroelectric properties of the sample were investigated by Piezoresponse Force Microscopy (PFM) in contact mode. PFM was used in writing mode in order to pole micron sized domains by applying various *DC* voltages on the tip (PFM-poling). The sample was connected to the ground during the writing procedure. We measured afterwards the PFM phase contrast (in reading mode). PFM imaging was carried out by applying on the sample a drive amplitude (*AC* voltage) of 4 V with respect to the tip.

The PFM-poled samples were characterized by Low Energy Electron Microscopy (LEEM) and by X-ray Photoelectron Emission Microscopy (X-PEEM). It has been already demonstrated that these two techniques are perfectly suited for imaging of ferroelectric domains.[21] LEEM close to the mirror mode was used to image samples after different poling procedures (PFM-poling and EC-poling) and XPEEM was used to spatially study the electronic structure of the PFM written patterns. Conventional XPS does not provide spatial information below the tens of micrometers scale, while X-PEEM gives simultaneously spectroscopic and microscopic information at scales that can reach tens of nanometers. In order to locate the PFM poled zone, we used samples with gold landmarks designed by laser lithography and we wrote a specific pattern by PFM-poling as shown on Figure 2(a). The white (respectively, black) regions correspond to a potential applied on the tip of +10 V (respectively, −10 V). Figures 2(c) and 3(a) show the LEEM image of the same region with two different fields of view. These images reproduce well the PFM phase image of Figure 2(b). After these measurements, the sample was +8 V EC-poled and reintroduced in the LEEM setup. Figure 3(b) shows the LEEM image of the same region as in Figure 3(a) but after +8 V EC-poling. We observe that the LEEM contrast at the previous PFM-poled zone has disappeared showing that +8 V EC-poling is sufficient to erase the +10/−10 V PFM-poled pattern. This means that the +8 V EC-poling procedure produces at the sample surface a voltage higher than the ferroelectric coercive voltage of the sample. We checked also that the ferroelectric properties of the sample were not altered after EC-poling by writing and reading a new PFM pattern in the same region.

X-PEEM was used to measure the photoemission threshold on a 15 nm $BaTiO_3$/Nb:$SrTiO_3$ sample on which a pattern was written by PFM with various poling potentials. The photoemission threshold corresponds to the lowest kinetic energy of electron experimentally reachable. To this aim, we

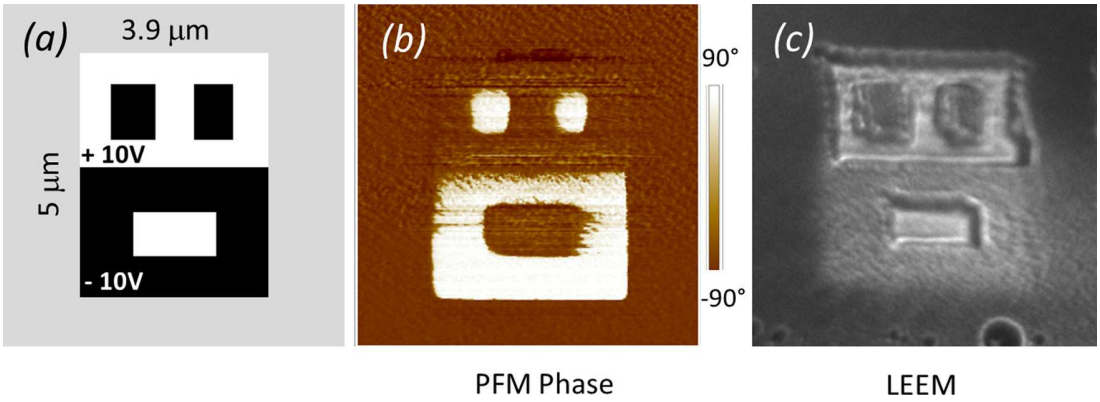

FIG. 2. (a) Pattern written by PFM on a 15 nm $BaTiO_3$/Nb: $SrTiO_3$(001). (b) PFM phase image after writing and (c) LEEM image of the same region for incident electron energy of 1.4 V.

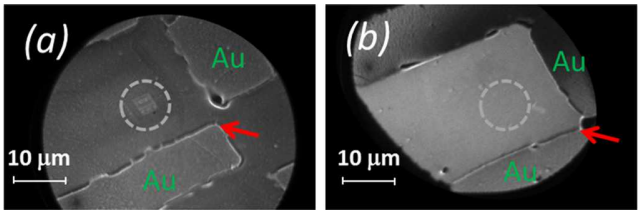

FIG. 3. LEEM image for an incident electron energy of 1.4 V on a 15 nm $BaTiO_3$/Nb:$SrTiO_3$(001) sample at the same region as in Fig. 2 (a) after PFM poling, (b) after PFM poling and +8 V EC poling. Gold landmarks are shown and red arrows and grey circles indicate the same place for the two images.

measured the photoemission signal by scanning the photoelectrons kinetic energy (from 2 to 8 eV) using an excitation photon energy of 200 eV. The photoemission threshold value is defined as the inflexion point of this curve. Using a local probe like XPEEM allowed comparative measurements of several sample regions poled with various potentials. The X-PEEM experiments were carried out on the I06 Nanoscience beamline at the Diamond Light Source, UK. Before analysis and in order to remove any surface contamination due to air exposure, the samples were outgassed in UHV at a temperature of 80 °C for 1 h. The XPEEM experiments were performed one week after the PFM writing.

The pattern written on the sample by PFM before X-PEEM investigations is plotted on Figure 4(a). The photoemission threshold map (Figure 4(c)) is obtained by calculating the photoemission threshold value for each pixel of the probed spatial area. The +10 V and −10 V PFM-poled regions appear as black and white, respectively, while the unpoled surface appears in grey. The curves on Figure 4(b) are the photoemission threshold spectra integrated on the different zones. The photoemission threshold for the +10 V (resp. −10 V) PFM-poled surface is lower (resp. higher) than the photoemission threshold for the unpoled surface. This means that a +10 V (resp. −10 V) PFM-poling induces a remnant electric field in the $BaTiO_3$ layer which decelerates (resp. accelerates) the outcoming photoelectrons with respect to the unpoled region. Such a negative shift in the position of the photoemission peaks was also observed by XPS for Ti-*3p* and Ba-*4d* core levels after +8 V electrochemical poling (with respect to the unpoled state). This demonstrates that the +10 V PFM-poling and the +8 V EC-poling induce the same remnant polarization direction.

We observe that +8 V EC-poling causes the same kind of photoemission peak shift than the well-known charging effect in conventional XPS, where exiting photoelectrons can be slowed down due to positive charges at the surface. This results in a shift of the photoemission peaks toward lower kinetic energies. In our case, the opposite effect consistently occurs for a −10 V PFM poling (shift toward higher kinetic energy). In addition, a +10 V (−10 V) PFM-poling is expected to create a downward (upward) remnant polarization, which is

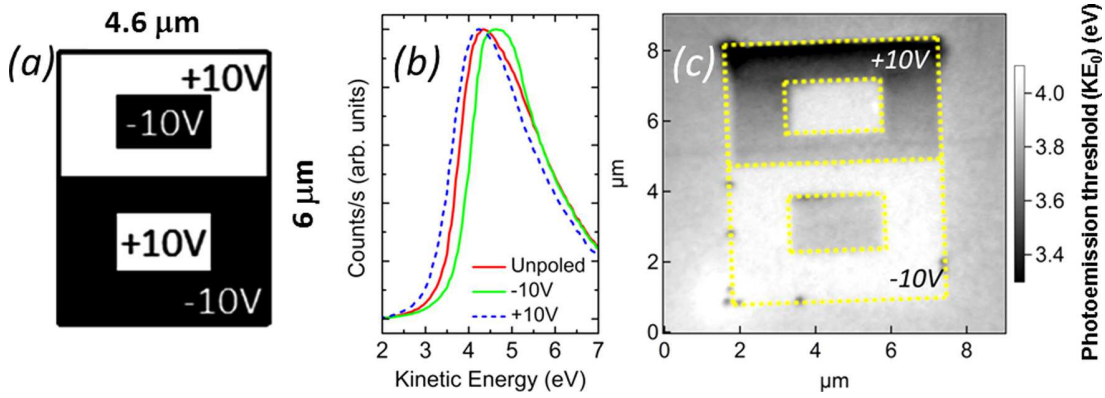

FIG. 4. (a) Scheme of the pattern written by PFM on a 15 nm $BaTiO_3$/Nb: $SrTiO_3$(001) sample. (b) Integrated photo-emission threshold spectra on unpoled (red solid line), −10 V (green solid line) and +10 V (blue dashed line) PFM-poled regions. (c) Photoemission threshold map.

subsequently screened at the sample surface by positive (negative) charges. Therefore, by comparing the sign of the charges, we can clearly conclude that the changes in the internal field recorded in XPEEM and XPS are due to the changes in the polarization screening charges.

In agreement with our experimental findings presented above, we can now understand the photocurrent improvement due to the +8 V EC-poling. Poling downward by applying a positive potential on the surface induces, through the polarization screening, an electric field that prevents electrons from the bulk to reach the surface, which is equivalent to attracting holes from the bulk to the surface, thus favoring oxidation reactions, i.e., oxygen evolution. This is consistent with previous studies where it has been demonstrated that photooxidation reactions occur preferably on downward polarized ferroelectric domains.[8–10,13] In the case of photoanodes, the objective is to realize water oxidation at the photoanode/electrolyte interface. This reaction involves a hole transfer from the photoanode to the electrolyte. Therefore, in order to increase the efficiency, it is desirable to drive the hole accumulation (i.e., the electron depletion) at the surface, which we managed to do thanks to the application of a positive poling potential. Here, we directly demonstrate the correlation between the physical phenomena induced by remnant polarization and photocurrent variations.

In conclusion, the effect of the internal electric polarization in an epitaxial ferroelectric based photoanode on the photocurrent was investigated by photocurrent measurements and correlated with PFM, LEEM and X-PEEM. We showed that the measured photocurrent is more than doubled when the ferroelectric layer is downward polarized. The substantial increase in the photocurrent is due to the existence of an internal electric field upon ferroelectric downward polarization which favors the displacement of holes to the surface where they can produce the water oxidation. Our study is a first step toward the tailoring of the photoelectrochemical properties through ferroelectricity. Such systems can serve as the next generation photoelectrodes within the framework of photovoltaics and water splitting applications.

This work was funded by the CEA and supported in part by Triangle de la Physique and Ile-de-France (C'Nano and ISC-PIF) under the IMAFMP grants.

[1]A. Fujishima and K. Honda, Nature **238**, 37 (1972).
[2]M. Gratzel, Nature **414**, 338 (2001).
[3]J. Han, Z. Liu, K. Guo, X. Zhang, T. Hong, and B. Wang, Appl. Catal., B **179**, 61 (2015).
[4]H. Magnan, D. Stanescu, M. Rioult, E. Fonda, and A. Barbier, Appl. Phys. Lett. **101**, 133908 (2012).
[5]I. Grinberg, D. V. West, M. Torres, G. Gou, D. M. Stein, L. Wu, G. Chen, E. M. Gallo, A. R. Akbashev, P. K. Davies, J. E. Spanier, and A. M. Rappe, Nature **503**, 509 (2013).
[6]Y. Yuan, Z. Xiao, B. Yang, and J. Huang, J. Mater. Chem. A **2**, 6027 (2014).
[7]D. Tiwari and S. Dunn, J. Mater. Sci. **44**, 5063 (2009).
[8]Y. Cui, J. Briscoe, and S. Dunn, Chem. Mater. **25**, 4215 (2013).
[9]J. L. Giocondi and G. S. Rohrer, J. Phys. Chem. B **105**(35), 8275 (2001).
[10]J. L. Giocondi and G. S. Rohrer, Chem. Mater. **13**, 241 (2001).
[11]N. V. Burbure, P. A. Salvador, and G. S. Rohrer, J. Am. Ceram. Soc. **89**(9), 2943 (2006).
[12]W. Ji, K. Yao, Y. C. Liang, and A. Suwardi, Appl. Phys. Lett. **103**, 062901 (2013).
[13]Y. Inoue, K. Sato, K. Sato, and H. Miyama, J. Phys. Chem. **90**, 2809 (1986).
[14]R. D. Nasby and R. K. Quinn, Mater. Res. Bull. **11**, 985 (1976).
[15]K. J. Choi, M. Biegalski, Y. L. Li, A. Sharan, J. Schubert, R. Uecker, P. Reiche, Y. B. Chen, X. Q. Pan, V. Gopalan, L.-Q. Chen, D. G. Schlom, and C. B. Eom, Science **306**(5698), 1005 (2004).
[16]A. Barbier, C. Mocuta, D. Stanescu, P. Jegou, N. Jedrecy, and H. Magnan, J. Appl. Phys. **112**, 114116 (2012).
[17]See supplementary material at http://dx.doi.org/10.1063/1.4930814 for RHEED stability measurements.
[18]N. Jedrecy, H. J. von Bardeleben, V. Badjeck, D. Demaille, D. Stanescu, H. Magnan, and A. Barbier, Phys. Rev. B **88**, 121409(R) (2013).
[19]D. Cao, Z. Wang, Nasori, L. Wen, Y. Mi, and Y. Lei, Angew. Chem., Int. Ed. **53**, 11027 (2014).
[20]J. Yin, J. Ye, and Z. Zou, Appl. Phys. Lett. **85**(4), 689 (2004).
[21]J. E. Rault, W. Ren, S. Prosandeev, S. Lisenkov, D. Sando, S. Fusil, M. Bibes, A. Barthelemy, L. Bellaiche, and N. Barrett, Phys. Rev. Lett. **109**, 267601 (2012).